Mon. Not. R. astr. Soc. (1980) **190**, 689–709

Neutral hydrogen and spiral structure in M33

K. Newton *Mullard Radio Astronomy Observatory, Cavendish Laboratory, Madingley Road, Cambridge CB3 OHE*

Received 1979 June 29; in original form 1979 June 5

Summary. Observations of neutral hydrogen (H I) in the galaxy M33 are presented which have sufficient angular resolution (47 x 93 arcsec) to distinguish detailed H I spiral structure for the first time. H I spiral features extend over the entire disc; the pattern is broken and multi-armed with the best-defined arms lying at radii outside the brightest optical features. Several very narrow spiral 'filaments' are unresolved by the beam, implying true widths $\lesssim 160$ pc. The H I is well correlated with other Population I material.

The only direct evidence for the presence of a density-wave in M33 is derived from the morphology of the inner southern arm. The radial velocity field, with resolution 16 km s^{-1}, is perturbed near the inner spiral arms. These perturbations agree with the predictions of density-wave theory but may simply arise from the self-gravity of massive arms whether or not they are a quasi-stationary wave phenomenon. If the outer spiral features form a rigidly rotating density-wave pattern, the absence of large radial streaming motions along the features implies a small pattern speed (< 25 km s^{-1} kpc^{-1}), with corotation in the outer parts of the disc.

1 Introduction

M33 is the nearest spiral galaxy with an inclination favourable for a study of its spiral structure. The first aperture synthesis survey of H I in M33 (Wright, Warner & Baldwin 1972; Warner, Wright & Baldwin 1973) was made with the Cambridge Half-Mile telescope at an angular resolution of 1.5 x 3.0 arcmin. More recently, Rogstad, Wright & Lockhart (1976) have mapped the central regions of M33 with an angular resolution (2.0 x 2.0 arcmin) similar to that of the Cambridge survey, but with greater sensitivity and radial velocity resolution. From studies of the optical composition of the bright southern arm, Dixon (1971) and Courtès & Dubout-Crillon (1971) found evidence for the presence of a density-wave, although Warner *et al.* put an upper limit of 3 km s^{-1} on streaming motions due to density-waves and Rogstad *et al.* found only weak evidence for streaming velocities within 12 arcmin of the nucleus. In addition, van der Kruit (1973) concluded from the absence of spiral structure in the 1415-MHz radio continuum distribution that there is little, if any, density-wave action in M33.

This paper presents a new survey made with the Cambridge Half-Mile telescope at an angular resolution of 47 x 93 arcsec, corresponding to ~ 160 x 310 pc in the plane of the sky at the distance of M33 (690 kpc, following Warner *et al.* 1973 and Rogstad *et al.* 1976). The radial velocity resolution is a factor of 2.4 better than the previous Cambridge observations and the sensitivity ($\Delta T_{\rm rms}$) over a single output map is improved by a factor of 4 at the same angular resolution.

2 Observations

Twelve-hour observations of M33 were made at 120 interferometer baselines from 12.2 to 737.6 m in 6.1-m intervals, providing maps with a maximum angular resolution of 47 x 93 arcsec. The envelope beam was centred within 40 arcsec of the position given by de Vaucouleurs, de Vaucouleurs & Corwin (1976) for the optical nucleus (RA $01^h\,31^m.05$; dec $30°\,23'.9$). The large-scale H I distribution, investigated by means of low-resolution maps from the small interferometer baselines, has been discussed elsewhere (Reakes & Newton 1978) with details of the observational procedure. Additional details regarding the high-resolution maps are given in Table 1.

The H I emission was measured over a 2-MHz bandwidth with a cross-correlation spectrometer. The output spectrum had a resolution of 16 km s^{-1}, centred on -210 km s^{-1}, and was sampled at values of radial velocity separated by 13.2 km s^{-1} to provide 32 output maps. Continuum radiation in a 10-MHz bandwidth, centred on 1420.0 MHz, was also measured.

Maps at 1.5 x 3.0 arcmin resolution were useful for some purposes and were derived from observations at 60 interferometer spacings. A correction was made for zero-level variation due to the absence of the spacings ($\lesssim$ 12.2 m) which cannot be reached by the 9.1-m diameter paraboloids, but the correction procedure (Newton 1978) does not restore to the maps any missing structure on a scale greater than ~ 1°. The maps with resolution 47 x 93 arcsec are not corrected for the missing spacings, since the resulting zero-level variation is small compared to the rms noise level. All maps *are* corrected both for aerial overlap on the 12.2-m spacing, and for radio continuum emission on the assumption that the H I optical depth is everywhere small. H I velocity profiles were constructed from the resulting maps of line emission and analysed to produce maps of integrated H I, radial velocity and velocity dispersion.

Table 1. Details of the observations.

Map Centre (1950.0)	
RA	$01^h\,31^m\,0^s.5$
DEC	$30^o\,24'\,00''$
Mean epoch of survey	1975.2
FWHP of primary beam	94 arcmin
Observed range of radial velocities	-2 to -411 km/s
Angular resolution	
60-spacing observations	1.5 × 3.0 arcmin
120-spacing observations	47 × 93 arcsec
Observed rms noise over single output map	
60-spacing observations	0.88 K
120-spacing observations	2.58 K

Positional accuracy was checked by comparing the positions of the six brightest sources on the broadband map at 47 x 93 arcsec resolution with corresponding positions from the survey by Israel & van der Kruit (1974). They agree to ± 1.5 arcsec. The sensitivity was calibrated by assuming 3C 286 to have a total flux density of 15.4 Jy and the flux density scale agrees with that of Israel & van der Kruit to ± 3 per cent.

Map coordinates are for epoch 1950.0 and radial velocities are heliocentric. At the assumed distance to M33 of 690 kpc, 5 arcmin corresponds to 1 kpc.

3 The high-resolution maps

Maps of integrated hydrogen (i.e. of $\int T_b \cdot dv$, where T_b is the brightness temperature of H I emission and the integration is over the range −55 to −319 km s^{-1} in radial velocity) were derived by addition of the line-emission maps. Signal-to-noise ratios were enhanced by (i) setting to zero values at all positions outside the region of detected emission on each output map before the addition, and (ii) by a gating procedure (e.g. Winter 1975) such that for each profile only those points with contributions exceeding 1.5 times the rms noise were included in the integration. The latter procedure has the disadvantage of underestimating low-brightness H I emission in the profile wings; the error is negligible for bright profiles if they are approximately Gaussian. Errors are most significant for low-brightness profiles, so the lowest contour (~ 3σ) shown on the maps of integrated H I will be underestimated by ~ 10–20 per cent, an effect still below the noise level.

It should be noted that zero levels of the maps would be affected by the absence of structure on a scale $\gtrsim 1°$ due to the missing interferometer spacings, but this is unlikely to be very significant (Reakes & Newton 1978).

Fig. 1 shows the integrated H I map at 1.5 x 3.0 arcmin resolution. It has a sensitivity ~ 6 times that of the earlier Cambridge map (Wright *et al.* 1972) but not as high as that of the survey by Rogstad *et al.* (1976); Fig. 1 extends, however, to much greater radii than the latter. It is in good overall agreement with both of these maps. At this resolution there is no *clear* overall spiral structure although, as noted by Wright *et al.* and Rogstad *et al.*, extended features are associated with the two major spiral arms indicated by the idealized spiral shown on Fig. 1. Emission to the extreme north and south of the figure is associated with the 'H I wings' described by Reakes & Newton (1978).

The output maps at 47 x 93 arcsec resolution contain much fine structure, with some unresolved features having brightness temperatures in the range 35–55 K. These temperatures are not much larger than the peaks observed by Rogstad *et al.* at lower resolution. The H I distribution in M33 is assumed to have small optical depth throughout the following discussion, but it should be noted that the true brightness temperatures and optical depths of unresolved features may be quite large. This is unlikely to alter significantly the conclusions of the paper.

Plate 1 shows a photographic representation of the 47 x 93 arcsec resolution map of integrated hydrogen, with emission integrated over the same range of radial velocities as before. The distribution now has a strikingly spiral appearance; there are several extremely narrow spiral segments with large ratios in projected density between the arm and interarm regions.

Fig. 2 is a more quantitative representation of the high-resolution map, while Plate 2 displays a representation of the approximate surface density in the plane of M33, based on the assumption that the H I lies in a thin disc inclined at 54° to the line of sight with the major axis in position angle 22°. Any finite thickness of the H I layer or warping of the disc will give rise to errors in this representation, although Reakes & Newton (1978) found no

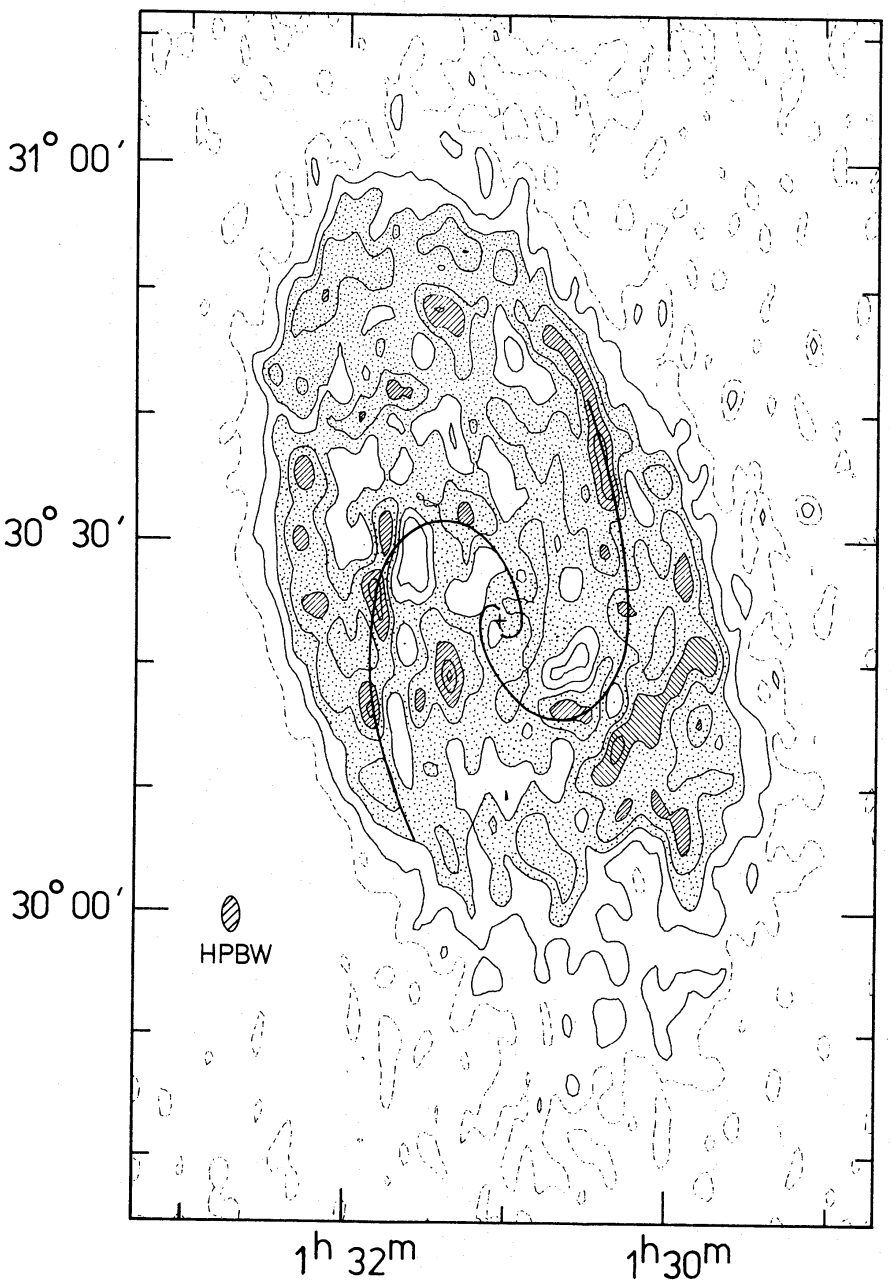

Figure 1. M33: Integrated hydrogen map at 1.5 × 3.0 arcmin resolution. The contour interval is 150 K km s^{-1} (≡ 2.7 × 10^{20} atom cm^{-2}, on the assumption of small optical depth) starting from 150 K km s^{-1}. The map has been corrected for the primary beam response, so the noise level rises towards the edge. The nucleus is marked by a cross, and the spiral curve is an idealized representation of the two major optical arms. Coordinates on this and other maps are for 1950.0.

evidence for distortion of the disc within R = 6 kpc, the approximate extent of emission on Plate 2.

4 Details of the H I distribution

4.1 THE OVERALL DISTRIBUTION

The mass of neutral hydrogen shown in Fig. 2 is ~ 75 per cent of that measured from the low-resolution (7 arcmin) maps of M33 by Reakes & Newton (1978), namely 1.0 × 10$^9 M_\odot$.

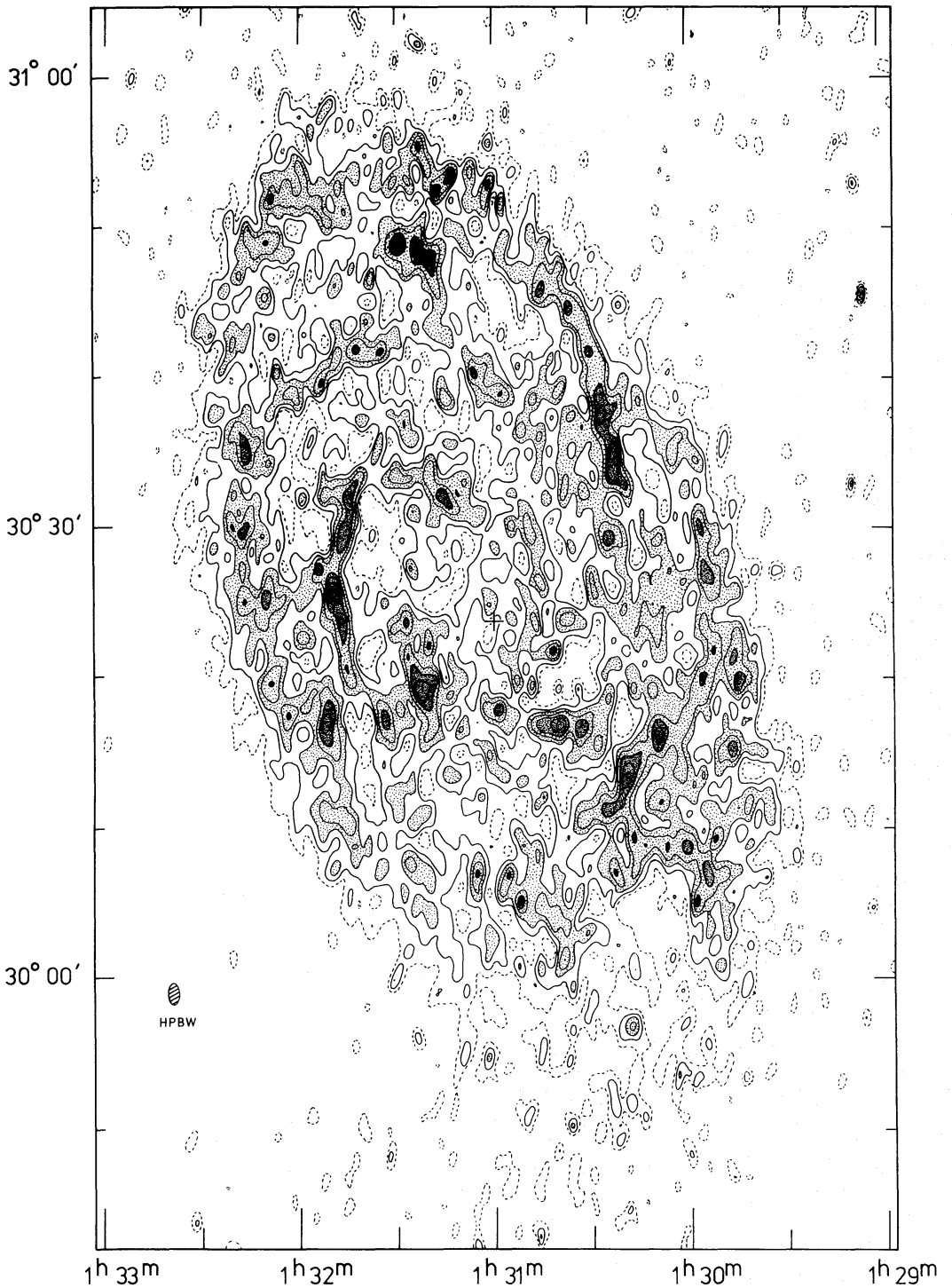

Figure 2. Contour map of the integrated H I emission from M33 at 47 × 93 arcsec resolution. The contour interval is 250 K km s^{-1} starting from 300 K km s^{-1}, and the rms noise is ≈ 100 K km s^{-1} at the map centre.

The difference is due mainly to the absence of extended emission having brightness comparable to the noise level, so falling below the first contour on Fig. 2 and to the gating procedure (Section 3). The difference between zero-levels of the two maps is small. The overall distribution is more organized than that seen in the previous high-resolution surveys, and the spiral features extend over considerable distances. On a smaller scale the H I is 'clumpy' and

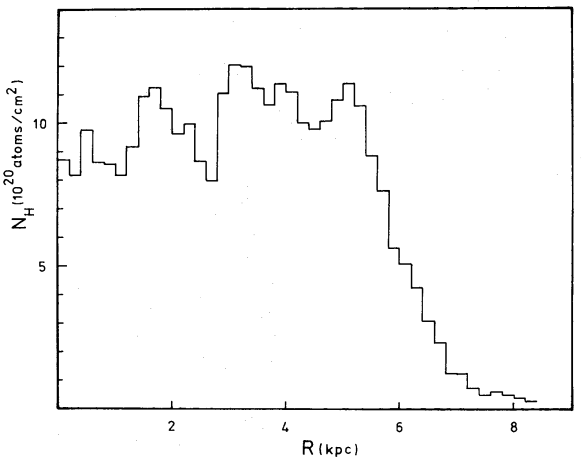

Figure 3. Mean surface density of H I as a function of radius in M33 obtained by integration in circular rings in the plane of the galaxy, assuming the p.a. of the major axis to be 22° and the inclination 54°.

even the spiral features generally consist of separate peaks joined by ridges of lower brightness emission, many features being still unresolved by the 47-arcsec beam. The brightest peaks on Fig. 2 have $\int T_b . dv$ values in the range 1400–2000 K km s^{-1}, which may be compared with the peaks of 1400 K km s^{-1} reached on the map with 1.5 x 3.0 arcmin resolution

The radial distribution of H I in M33 is shown in Fig. 3, obtained by averaging emission on Fig. 2 over circular annuli in the plane of the galaxy. Comparison with Fig. 6 of Wright *et al.* (1972) shows that there is more structure in the new curve for $R < 3$ kpc, with a minimum at $R = 2.6$ kpc, where the average emission is 30 per cent lower than at adjacent radii. This minimum coincides with the radius at which emission from the inner arms dies away. For $3 < R < 5$ kpc, the distribution has a fairly constant value of 1.1×10^{21} atom cm^{-2} normal to the plane of the galaxy, and there is a sharp cut-off beyond 5 kpc.

4.2 SPIRAL STRUCTURE

Spiral features extend over the entire disc to $R \sim 6$ kpc and they are trailing if the usual assumption is made, that the north-west edge is the nearest. Although several spiral 'segments' are very well defined in Plate 1, superposition of the two halves of the map, rotated about the nucleus, reveals no overall symmetrical spiral pattern. If the rotation is carried out about a point 1.6 arcmin northwards from the nucleus along the major axis, the *symmetry* is improved, but there remains no uniquely defined spiral *pattern.*

Several spiral features are very narrow in relation to their separation. In many places they are unresolved, implying true widths less than ~ 160 pc. In the density-wave picture, narrow H I arms may arise from compression of the gas by a shock front at the edge of a spiral arm (e.g. M81, Visser 1978). However, it has been deduced on kinematical grounds that only weak shocks, if any, are possible in M33 (Roberts, Roberts & Shu 1975), a result consistent with the appearance of the generally broad, patchy and poorly defined optical arms. The existence of very narrow spiral features in the H I distribution is therefore surprising; their relation to the radial velocity field is discussed in Section 6.

In order to facilitate the following discussion, Fig. 4 shows a sketch of the clearest spiral features, numbered for ease of reference. Consider the maps (Plates 1 and 2, Fig. 2) in two parts.

(i) $R < 12$ arcmin: This area (within the inner circle shown on Plate 2) contains the two brightest and best-defined optical arms, indicated by the spiral curves on Fig. 1, of which the

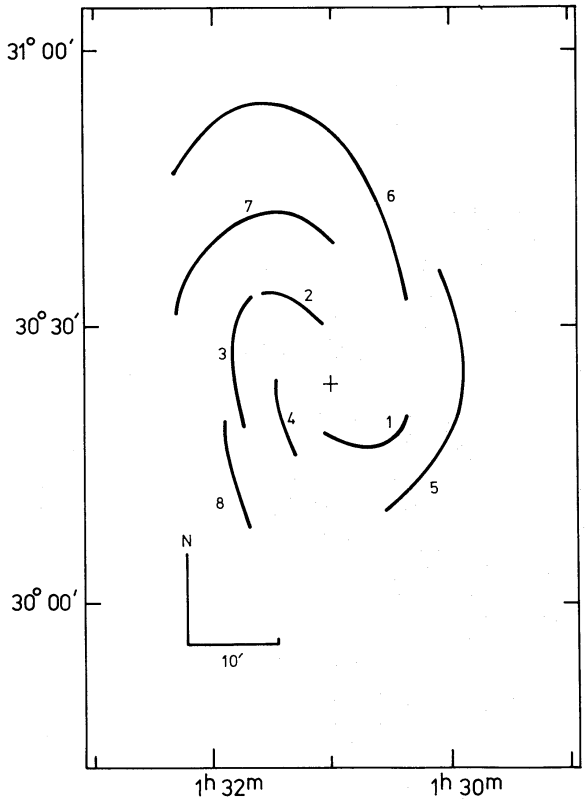

Figure 4. Sketch indicating prominent spiral features in the distribution of integrated H I emission from M33 shown in Plate 1.

southern arm is the most prominent. The same is not true of the H I distribution; although the 'southern arm' contains some of the brighter H I emission, there are better defined and brighter H I arms elsewhere. Features 1 and 2 on Fig. 4 are the corresponding H I arms, which may be traced from $R \sim 6$ arcmin. The southern arm is the clearer and brighter of the two, but both lie close to the spiral curve with pitch angle $\sim 27°$ derived from optical measurements. In addition there is a bright extended H I complex in the south-east quadrant at $R \sim 10$ arcmin (feature 4) which may be a subsidiary arm; low-brightness H I emission in the north-west (RA $01^h\,30^m\,40^s$, dec $30°\,26'$–$30°\,31'$) may form a symmetrical, but much less distinct feature.

The average arm–interarm density–contrast ratio observed along the southern arm is $\sim 2.5{:}1$, and reaches 7:1 for the brightest ridge. The northern arm is less well-defined, having an average contrast ratio of $\sim 2{:}1$. The gating procedure and any variation in zero-level due to missing large-scale structure would decrease measured contrast ratios, but such effects are probably small (Section 3). In addition, true contrast ratios could be even greater, since H I may be optically thick in dense concentrations, and the compression regions of the gas in unresolved spiral features may be on still smaller scales.

(ii) $12 < R < 30$ arcmin: The spiral pattern in this region is clearly multi-armed. Several features e.g. 5 and 7, have smaller pitch angles ($\sim 20°$) than the inner arms. H I spiral features are clearest in the northern half of M33 and they extend further from the nucleus than in the south. This may be another reflection of the asymmetry noted in previous surveys: although the brightest emission occurs in the south-west quadrant of the central disc, H I emission from the north-west 'wing' in the outer parts is brighter than in the south-east (*cf.* Reakes & Newton 1978). The spiral features at the edge of the disc in Fig. 2 merge to give the impression of a narrow ring of emission, particularly down the eastern side.

The inner northern arm (2) dies away at $R \approx 12$ arcmin but continues at greater radii (feature 3) and extends southwards for 3 kpc. This part of the arm is well-defined and generally unresolved in width. There is no corresponding extension to the inner southern arm, but feature 6, beginning at $R \approx 20$ arcmin may be a continuation, having a similar pitch angle of $\approx 27°$. Both features have high contrast ratios, typically 3.3 : 1. Contrast ratios observed in the present survey are considerably higher than those found before.

It is concluded that the spiral structure in the outer parts of the disc is broken and contains at least four separate arms, although these features are not consistent with the four-armed spiral pattern derived by Boulesteix *et al.* (1974) from the earlier Cambridge H I map at 1.5 arcmin resolution.

5 Relationship between H I and other Population I material

5.1 DUST

The H I is well correlated with the few conspicuous dust features in M33. Dust lanes (Plate 3) run along the inside of the bright southern optical arm, coinciding with H I peaks towards the end of the arm; features to the immediate west and south of the arm are also concomitant with extended H I. Several dust features are visible on the outside edge of the northern arm, with a particularly sharp feature close to the nucleus, and more to the west of the arm. These features are again well correlated with peaks of H I emission. Detailed correlation between neutral hydrogen and dust is well established for several other spiral galaxies e.g. M31 (Emerson 1974) and M81 (Rots & Shane 1975), but is a new result for M33.

5.2 STELLAR SPIRAL STRUCTURE

5.2.1 Morphology of the inner arms

The two prominent optical arms extend to a radius of 12 arcmin, their brightness decreasing markedly thereafter. The southern arm is well defined by stars and the inner side is particularly clear, having a remarkably sharp chain of very small and intense H II regions (Boulesteix *et al.* 1974). This chain has been interpreted as marking the position of a shock-front (Dubout-Crillon 1977 and references therein). A series of dust lanes running along the inside of the arm emphasizes the feature. Dubout-Crillon has carried out a detailed investigation of the arm and presented evidence for the propagation of the locus of star formation through the galactic material. She compared the optical data and the earlier Cambridge H I survey, and found the peaks of neutral hydrogen to lie along the inner part of the arm but outside the H II chain.

The present survey confirms that peaks of H I lie along the inside edge of the southern arm (Plate 3) and shows the H I ridge to be extremely narrow ($\lesssim 300$ pc) in comparison with the stellar arm which is 600–800 pc across. Plate 4 shows H I contours superimposed on an Hα photograph of the arm (Dubout-Crillon 1977). The H I is roughly coincident with the chain of small H II regions noted by Boulesteix *et al.* On a smaller scale, H II regions within $R = 7$ arcmin are generally on the inside edge of the H I peaks (labelled A and B on Plate 4), but for $R > 7$ arcmin the H II chain is apparently displaced to the outside of the H I ridge (C). The coincidence of the H I with dust lanes between $R = 7$ and $R = 12$ arcmin may indicate that some H II regions are obscured. The overall association of H I with dust and H II regions along the inside edge of the southern arm is consistent with predictions of the 'non-linear' density-wave theory (Roberts & Yuan 1970) where a shock, a non-thermal radio-continuum peak, dust lanes and H I peaks are expected to lie in a narrow compression

Figure 5. Distribution of integrated H I emission in M33 at 47 × 93 arcsec resolution, together with the positions of classical H II regions taken from Boulesteix *et al.* (1974). Small crosses indicate H II regions of low intensity (class 1 and 2 as defined by Boulesteix *et al.*) and dots indicate brighter regions of intensity class 3 and 4. Large crosses show the positions of 'ring' H II regions and the shading indicates their approximate extent. The contour interval is 500 K km s^{-1} starting from 750 km s^{-1}.

region on the inside edge of the optical arm, if the arm lies within the corotation radius (at which the density-wave pattern speed is equal to the rotation velocity of the gas). This is also reflected in the radio-continuum distribution; although Israel & van der Kruit (1974) observed no spiral structure at 1415 MHz, von Kap-herr, Berkhuijsen & Wielebinski (1978) found extended emission associated with the inner spiral arms at 4850 MHz. Their map at 2.6-arcmin resolution shows a ridge of emission towards the end of the southern arm coincident with the H I peak (C) and lying on the inside edge of the optical emission. It is not yet clear, however, what fraction of this emission is non-thermal.

The present observations are therefore in agreement with the evidence provided by Dubout-Crillon (1977) that a shock-front, associated with a density-wave, can explain the morphology and the organized star formation observed in the southern arm. She also concluded on kinematical grounds that a shock is not expected in the northern arm. Star formation is more random in the northern arm and Plate 3 shows the northern arm not to be so well-defined as the southern, either optically or by the H I. Here the bulk of the optical emission lies along the inside edge of the H I peaks, although several H II regions are associated with the H I ridge itself (Fig. 5). There is extended radio-continuum emission associated with the inner part of the arm (von Kap-herr *et al.* 1978), but this is coincident with the optical emission lying inside the H I peaks. This morphology does not suggest the presence of a shock associated with the northern arm and moreover, if the arm lies inside the corotation radius as assumed for the southern arm, the displacement of H I to the outside of the optical emission is apparently in conflict with a density-wave explanation. The structures of the two inner arms differ significantly, and a more detailed study of the Population I material and the age distribution of stellar material across the northern arm is needed before the situation can be clarified.

5.2.2 The outer arms

The northern H I arm continues as far as the giant H II region NGC 604 (Fig. 5), and thence extends southward for ≈ 15 arcmin. This part of the arm contains relatively strong H I emission, but there is little optical emission associated with it; the H I ridge lies outside the central area of bright optical emission (Plate 3). This effect may be at least partially due to the presence of dust, since there is a marked drop in the background optical emission along the H I ridge. A large H I 'cloud' in the south-west was noted in both previous aperture synthesis surveys; it contains considerable fine structure at 47 x 93 arcsec resolution, and the peaks along the front edge of the feature delineate a spiral segment (labelled '5' on Fig. 4). Correlation between H I and optical emission in the outer parts of M33 can be seen more clearly in Plate 5.

It may be noted that down the eastern side of the galaxy, several optical features run almost orthogonal to H I features, and some have no apparent counterparts in the neutral hydrogen distribution. In general, however, H I peaks are very well correlated with the optical peaks. Preliminary comparisons of the H I data with new measurements of the distribution of blue supergiant stars in M33 (Madore 1978) show a good correlation over the entire disc.

5.3 H II REGIONS

Although Wright *et al.* (1972) found no strong correlation between the projected H I density of their H I map and the positions of the 10 brightest H II regions in M33, Israel & van der Kruit (1974) found a very pronounced tendency for H II regions, detected by radio continuum emission, to lie in places of high H I surface density. This was confirmed by Madore, van den

Bergh & Rogstad (1974) by a quantitative study of the correlation between a sample of 309 H II regions and the Owens Valley H I map at 2-arcmin resolution. The linear scale over which data are averaged is an important factor to be considered in such comparisons (e.g. M31, Emerson 1974; Unwin, in preparation). The greater angular resolution of the present survey allows the correlation to be extended to a smaller linear scale.

Fig. 5 shows the new H I distribution, together with the positions of classical H II regions taken from Boulesteix *et al.* (1974). The overall correlation is remarkable, and H II regions are closely associated with H I spiral structure in the outer parts of the galaxy. In the inner part of M33 the H II regions are concentrated towards the centre. In the central region, $R < 2.4$ kpc, there are no H II regions if the H I emission is below 250 K km s^{-1} (8.3 per cent of the area involved) and only 7 where the H I emission is less than 400 K km s^{-1} (20 per cent of the area), from a total of 171 regions. The correlation was investigated further for two concentric areas in the plane of M33, centred on the nucleus: (i) the inner region for $R < 2.4$ kpc and (ii) the outer region for $2.4 < R < 4.8$ kpc, assuming an inclination of 54° and major axis p.a. of 22° as in Plate 2. An analysis similar to that described by Madore *et al.* (1974) was carried out by considering the average number-surface-density of H II regions within different ranges of integrated H I emission. The 'ring' H II regions marked on Fig. 5 and discussed below were omitted from the analysis, as were the giant regions NGC 604 and NGC 595.

If the observed number of H II regions is assumed to be proportional to the rate of star formation, this leads to a relationship between the surface densities of H I ($\sigma_{\rm HI}$) and of H II regions ($\sigma_{\rm HII}$) of the form

$$\sigma_{\rm HII} \propto \sigma_{\rm HI}^{n}$$

(e.g. Madore *et al.* 1974 and references therein). Plots of log (H II surface density) against log (H I surface density) for the two areas defined above are shown in Fig. 6. Fig. 6(a) indicates $\sigma_{\rm HII}$ to be only weakly (if at all) dependent on $\sigma_{\rm HI}$ in the inner area; there are no H II regions for $\sigma_{\rm HI} < 4.8 \times 10^{20}$ atom cm^{-2} and the initial rise of $\sigma_{\rm HII}$ flattens at large $\sigma_{\rm HI}$ values. Assuming the above power-law relation, a weighted least-squares fit to Fig. 6(a) yields a value of $n = 0.6 \pm 0.1$ for $\sigma_{\rm HI} > 4.8 \times 10^{20}$ atom cm^{-2}, which is appreciably lower than the overall value $n = 0.91 \pm 0.14$ derived by Madore *et al.* for the same area. Within this inner region, there is a tendency for H II regions to cluster *around* the stronger H I peaks, an effect especially clear in the southern arm. This small-scale anticorrelation is manifested on Fig. 6(a) by the apparent saturation at high values of $\sigma_{\rm HI}$, i.e. there is no increase of the density of H II regions with H I column density above 2.3×10^{21} atom cm^{-2}. A similar effect was found by Madore *et al.*, who suggest that extinction by interstellar dust in regions of high H I density can account for the observed saturation. Dubout-Crillon (1977), however, noted the presence of large areas of diffuse Hα emission in the arms and concluded that it is unlikely that dust and molecular clouds *prevent* the detection of H II regions with high emissivity inside the arms, but *let through* faint, diffuse emission. The present survey has shown that some H I peaks for which the 'saturation' effect is clearest are coincident with dust features; it therefore seems probable that extinction will indeed be important in these areas.

Fig. 6(b) is based on the distribution of a further 154 H II regions in the outer area. The gradient is much steeper, with a value of $n = 2.0 \pm 0.1$, which is again lower than the value $n = 2.57 \pm 0.24$ derived by Madore *et al.* from the lower resolution H I data over a similar area. There are several systematic effects which are probably larger than the indicated random errors and which complicate the interpretation of these comparisons. In addition to the obscuration by dust, (i) considerable amounts of gas, especially in the central regions, may be present in molecular or ionized forms (ii) many H II regions have relatively large

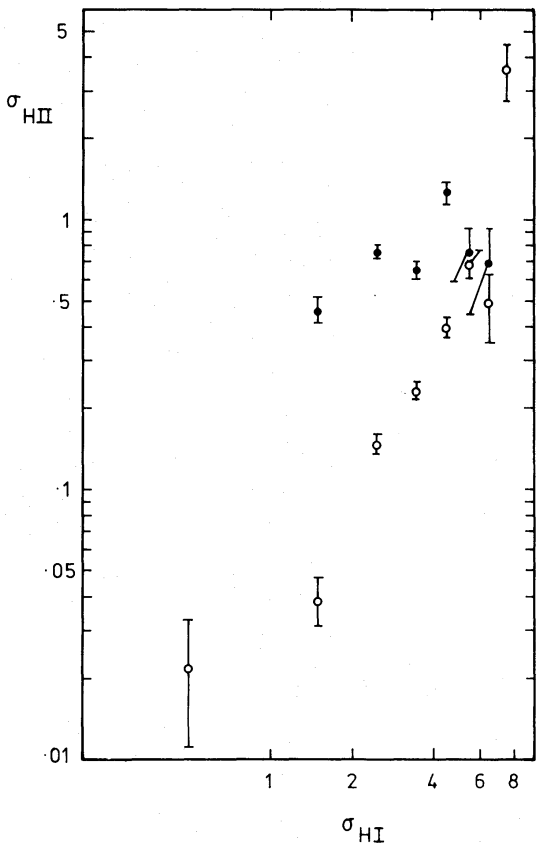

Figure 6. Relation between observed line-of-sight density of H I, in units of 4.6×10^{20} atom cm^{-2}, and the number density of H II regions (number per square arcmin). (a) Inner region $0 < R < 2.4$ kpc: Filled circles. There are no H II regions for $\sigma_{HI} < 4.6 \times 10^{20}$ atom cm^{-2}. (b) Outer region $2.4 < R < 4.8$ kpc: Open circles.

angular sizes and cover a range of H I emission, (iii) the gating procedure applied to the new map (Section 3) affects the calculated value of σ_{HII} at the lowest σ_{HI} values, and (iv) any error in the zero level of the H I map due to missing large-scale structure would increase the derived value of n. It is unlikely that the latter effect is important, since little structure on a scale larger than 1° is expected (Reakes & Newton 1978). The gating procedure is unlikely to shift the first point on Fig. 6(b) to the right by more than 100 K km s^{-1}, which would increase n to 2.1 ± 0.1. There is evidence that values of n derived for M31 decrease with increasing linear resolution of H I observations down to a scale of $\sim 200 \times 800$ pc in the plane of the galaxy (Emerson 1974; Unwin, in preparation).

For M33, although the new result is lower than that by Madore *et al.*, there are possible systematic effects and the difference is not very significant; the value $n \sim 2$ for the outer region is maintained down to a scale of at least 220×370 pc in the plane of the galaxy. This value may be compared with values between 1.8 and 3.5 found for several other galaxies over a range of linear scales from 0.2 to 5 kpc (summarized by Berkhuijsen 1977). The saturation effect at high σ_{HI} values is not so apparent in the outer parts of the disc; although H II regions in some parts of Fig. 5 surround H I peaks, in other parts they coincide with the peaks. This is especially clear near features 3 and 6, which contain some of the brightest emission on the map. NGC 604, often believed to lie outside the northern arm, in fact is on the H I ridge forming an apparent extension to the inner optical arm.

The 13 'ring-like' H II regions noted by Boulesteix *et al.* are shown, with their approximate extents, on Fig. 5. These regions have diameters between 100 and 270 pc, and it is not clear

whether they are annular filaments or spherical shells. Boulesteix *et al.* suggest that they represent late stages in the lives of expanding ionized regions. Since the diameters are significant when compared both to the width of the H I spiral features and to the thickness of the H I layer (*cf.* Warner *et al.* 1973), we might expect to find detectable effects in the H I distribution. Many of the regions are associated with H I spiral features (Fig. 5) and some with irregularities in the surrounding H I emission. Effects are particularly noticeable around the rings at RA $01^h\,29^m.77$, dec 30° 24′.7 and RA $01^h\,31^m.39$, dec 30° 55′.0, (labelled A and B on Fig. 5) where there are central H I depletions and enhancements of emission around the outside. Conversely, there are other cases where the rings apparently surround an H I *peak*, e.g. at RA $01^h\,29^m.92$, dec 30° 9′.5 and RA $01^h\,31^m.71$, dec 30° 41′.9 (C and D).

6 The radial velocity field

A radial velocity was assigned to each profile by taking the mean of the two velocities at which intensities had dropped to 0.5 of the peak value. Warner *et al.* (1973) discuss the accuracy with which velocities may be determined.

Plate 6 shows the radial velocity field at 47 x 93 arcsec resolution superposed on the map of integrated H I. The overall pattern of differential rotation is clear, and considerable fine structure is visible, although much of this is attributable to the rms noise level which is typically 2–4 km s^{-1}. A useful aid in the search for systematic velocity-perturbations associated with the spiral arms is a 'residual velocity' map produced by the subtraction of a model velocity-field, involving circular rotation, from the observations. An estimate of the equilibrium rotation curve is required in order to produce such a model; provided that the rotation curve is reasonably smooth, residuals corresponding to perturbations on the scale of the spiral arms should then become apparent.

6.1 ROTATION CURVE

Better estimates of the *average* disc parameters can be derived from a radial-velocity map at 1.5 x 3 arcmin resolution, for which the velocity distribution is more continuous than at higher resolution. Values of p.a., inclination and systemic velocity derived from such a map are in excellent agreement with previous determinations, and the following values are adopted:

major axis p.a. = 22°,
inclination = 54°,
$V_{sys} = -180$ km s^{-1}.

The rotation centre coincides with the assumed position of the optical nucleus to within ≈ 30 arcsec. The rotation curve shown in Fig. 7(a) was derived from the same map, by averaging velocities in circular annuli in the plane of M33. Velocities close to the minor axis were given zero weight, and the errors were derived from the scatter of values within each annulus.

Major-axis rotation velocities derived from the radial-velocity map at 47 x 93 arcsec resolution are shown in Fig. 7(b), assuming the disc parameters given above. The maximum difference between Fig. 7(a) and (b) at any radius is only 10 km s^{-1}. The smooth curve in Fig. 7(a) was used to calculate a model radial-velocity field, which was then subtracted from the observed velocity field at 47 x 93 arcsec resolution to produce the map of residual velocities in Plate 7. The residuals are generally small, with values rarely exceeding 10 km s^{-1}.

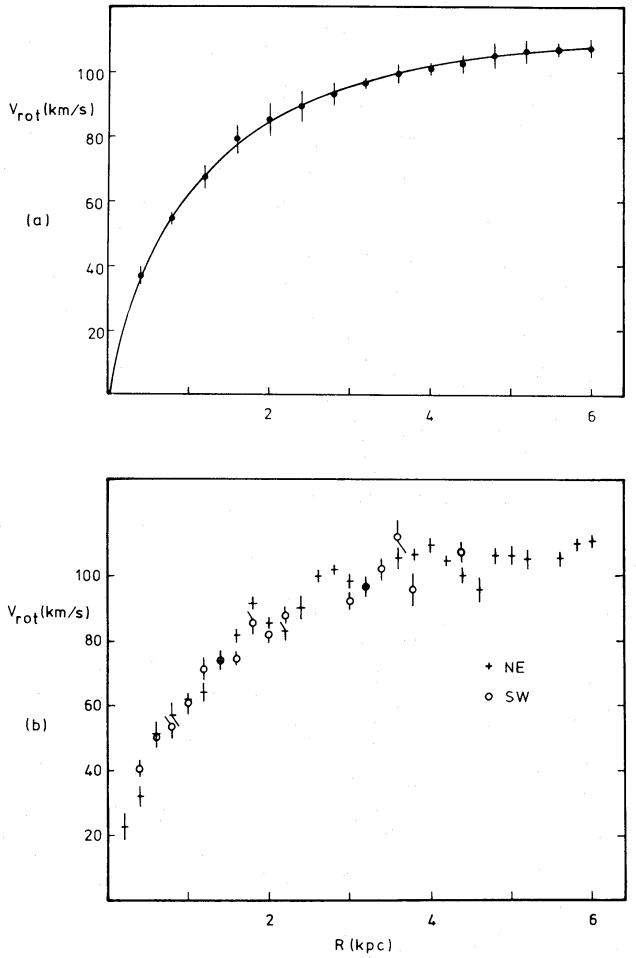

Figure 7. Rotation velocities of H I gas in M33, derived as described in the text: (a) from the radial-velocity field at 1.5 X 3.0 arcmin resolution, (b) major-axis rotation velocities derived from the radial-velocity field at 47 X 93 arcsec resolution.

6.2 COMPARISON WITH THE PREDICTIONS OF DENSITY-WAVE THEORY

A feature in M33 initially extended radially between $R = 3$ and $R = 5$ kpc would, after 3×10^8 yr (two rotations at $R = 5$ kpc), be drawn by differential rotation into a spiral shape of length ~ 20 kpc and with pitch angle < 20°. Further, the 'winding rate' varies across the disc. Therefore, if individual spiral features in M33 are transient but overall spiral structure is a long-lived phenomenon, a regenerative process needs to be invoked which can account for the presence of many spiral features, typically 4 kpc in length and having similar and relatively large pitch angles across the entire disc at the current epoch. In addition, if the H I features are material arms, it is difficult to explain their very narrow widths. The explanation of spiral structure as a wave phenomenon, where the overall pattern is long-lived and galactic material rotates *through* the arms, is therefore attractive.

Recent reviews of density-wave theories and their confrontation with observations are presented by Toomre (1977) and Kalnajs (1978). The poor definition of spiral structure in M33 has been explained in the context of the density-wave theory as a consequence of the fact that only weak shocks, if any, are capable of propagation in this galaxy (e.g. Roberts *et al.* 1975). Previous comparisons between observed radial velocities in M33 and the predictions of density-wave theory have been made by using the formulae derived by Lin, Yuan & Shu (1969), and assuming a two-armed logarithmic spiral pattern with pitch angle ~ 30° (e.g.

Warner *et al.* 1972; Rogstad *et al.* 1976; Newton 1978). These models are based on the linear (i.e. shock-free) density-wave theory. It is important to note that (i) the present survey shows the H I spiral structure to be broken, with no overall symmetrical pattern, and (ii) Lin *et al.* assume a tightly-wound spiral, which is not the case in M33. However, if a two-armed 'grand-design' density-wave pattern dominates the dynamics of the gas anywhere in M33, we might expect it to be in the inner region ($R < 2.4$ kpc), where the two major optical arms are found and weak evidence for density-wave perturbations was found by Rogstad *et al.* (1976). The response of the gas to the linear density-wave is such as to produce an *apparent* radial motion inward toward the nucleus within an arm, and an outward motion in interarm regions, with the directions of these motions reversed beyond the corotation radius. The tangential component of the response is such as to increase rotational velocity on the outside edge of a spiral arm, and to decrease $V_{\rm rot}$ on the inside edge. In principle, the pattern speed may be derived from the phase of the perturbations. The analysis carried out by Rogstad *et al.* showed good agreement between the signs of observed and predicted residuals for $R < 12$ arcmin, and the best fit to their radial velocity field gave the corotation radius as 1.4 kpc (= 7 arcmin).

In the present survey, the signs of observed residuals in Plate 7 also show agreement with the predictions of density-wave theory in the central region ($R < 2.4$ kpc) near the major axis, where the clear H I spiral features occur. The agreement is best near the southern arm; residuals correspond to peaks in rotation velocity outside the arm, with a corresponding decrease of $V_{\rm rot}$ along the inside edge (peak-to-peak magnitude 12 km s^{-1}). Fig. 8 is a more

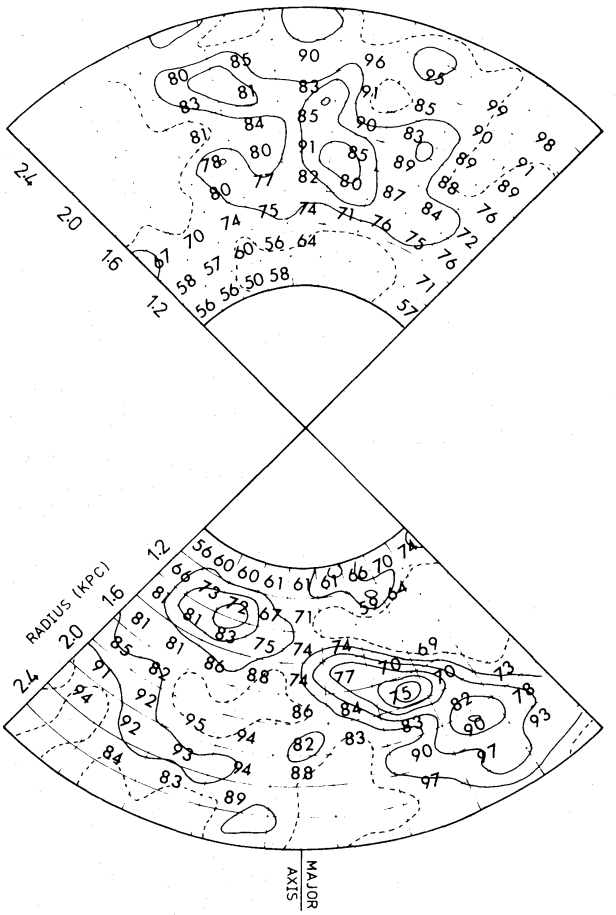

Figure 8. $V_{\rm rot}$ (R, θ) measured in the plane of M33 at intervals of 0.2 kpc in R and 10° in θ. Contours are of $\int T_{\rm b} \cdot dv$; dashed contour 500 K km s^{-1}, interval 250 K km s^{-1}.

quantitative representation, showing rotation velocities measured around concentric circles in the plane of the galaxy. Rotation velocities are derived from the observed radial-velocity field, assuming the disc parameters given in Section 6.1. There is a clear increase in rotation velocity at constant radius across the southern arm (e.g. at R = 20 kpc, the rotation velocity increases from 73 km s^{-1} in the west on the inside of the arm to 83 km s^{-1} in the east on the outside), an effect similar to that noted by Dubout-Crillon (1977) from optical velocity measurements. The effect is less apparent for the northern arm, but there is a general increase in V_{rot} towards the outer edge of the arm on Fig. 8 between R = 1.6 and R = 2.4 kpc, and residuals around the outside of the arm near the major axis (Plate 7) are generally negative, corresponding to an average increase in rotation velocity. It is not possible to confirm the weak evidence found by Rogstad *et al.* (1976) for density-wave perturbations near the minor axis, within R = 2.4 kpc, since in the present survey the velocity field over the rest of this inner region is not continuous, and most observed residuals are not significantly greater than the rms noise. In addition, residuals are found near the bright H I complex in the south-east (feature 4 on Fig. 4) which are large and apparently unsystematic.

No estimate of corotation radius may therefore be made from the velocity field within 2.4 kpc of the nucleus in the present survey, since the only systematic perturbations observed are tangential, and the sign of the perturbations is not affected by the choice of pattern speed. Further, we expect (qualitatively) to find such perturbations near a spiral arm *whether or not* it is a quasi-stationary wave, due to the 'self-gravity' of the arm. Perturbations (largely tangential) would arise from the additional gravitational acceleration produced by the excess mass in the arm. If the effects of optical depth are small, self-gravity of the H I gas alone cannot explain the perturbations; the significance of the self-gravity effect therefore depends upon the distribution of the rest of the material in the arm. The observed velocity perturbations occur across the H I ridge which lies along the inside of the much broader optical arm. In view of the dust lanes coincident with the H I ridge, it is likely that there is a considerable mass of Population I material associated with this part of the arm, in which case self-gravity may indeed explain the perturbations.

The northern arm is less massive, as may be seen both from the H I observations and from its optical appearance. The effect of self-gravity on rotation of the gas would therefore be of smaller magnitude, consistent with the observations. These observations of radial velocities in the central regions of M33 therefore provide no *conclusive* evidence for agreement with the density-wave theory although, in view of the morphological evidence for the presence of a density-wave in the southern arm and the association of observed velocity perturbations with the postulated shock-front, a density-wave explanation seems likely for this feature at least.

6.3 PERTURBATIONS IN THE RADIAL COMPONENT OF VELOCITY

If density-wave perturbations are present in the velocity field, the observations of *radial* streaming motions would enable a more conclusive comparison with theory to be made. Radial motions have a maximum observable effect near the minor axis, but emission from the southern arm dies away near the major axis. The extension to the northern arm (3) reaches larger radii, but there are no apparent *systematic* perturbations of the form expected from density-wave models, and the rms noise of 2–3 km s^{-1} for radial velocities measured along the H I ridge may account for the variations which are seen. There are also no apparent systematic velocity-perturbations associated with the spiral features in the outer parts of the disc. Residuals typically reach 5 km s^{-1}. They exceed 10 km s^{-1} in places, but the effects

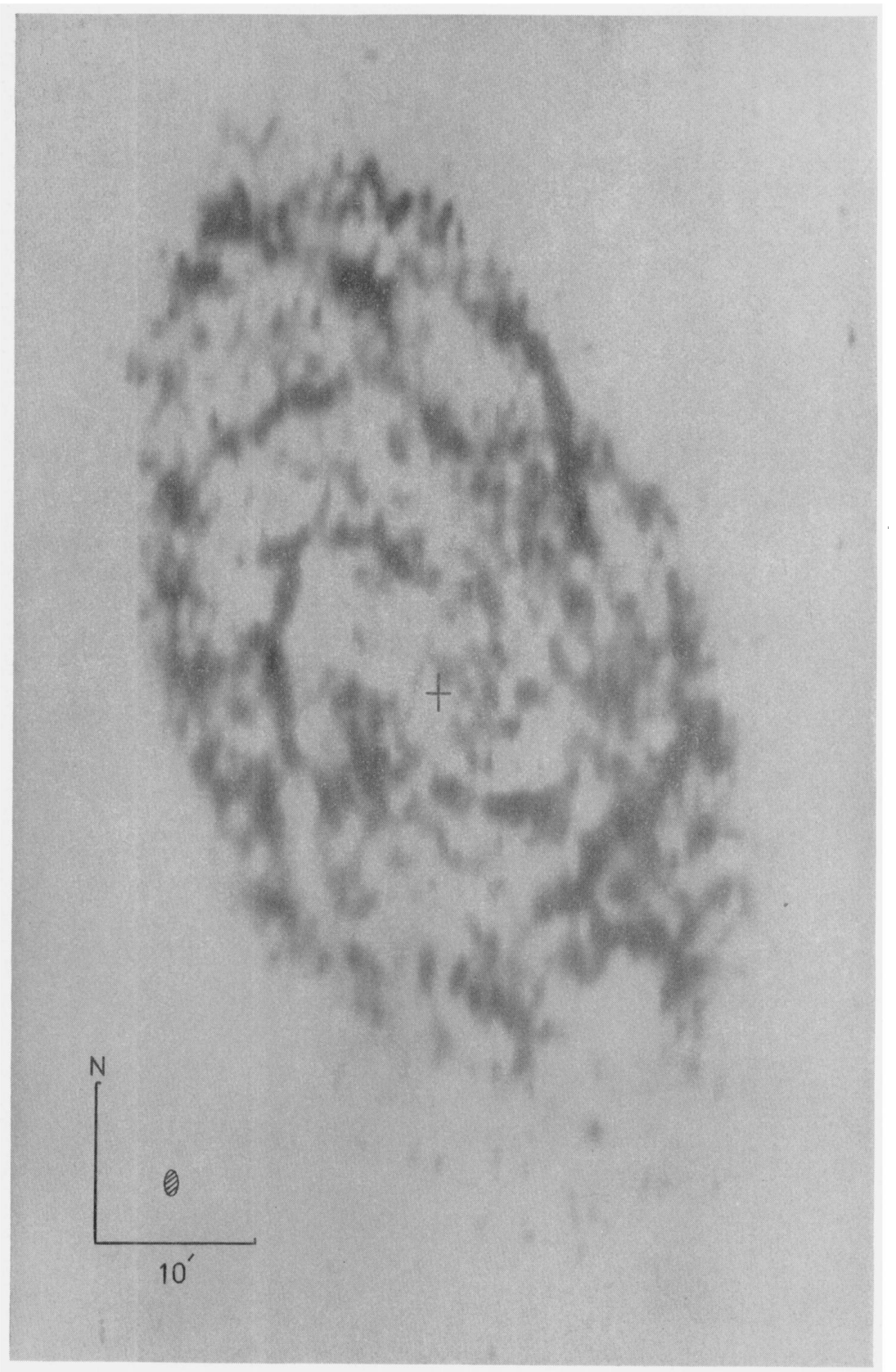

Plate 1. A photographic representation of the integrated H I emission from M33 at 47 × 93 arcsec resolution. The nucleus is marked by a cross.

[*facing page* 704]

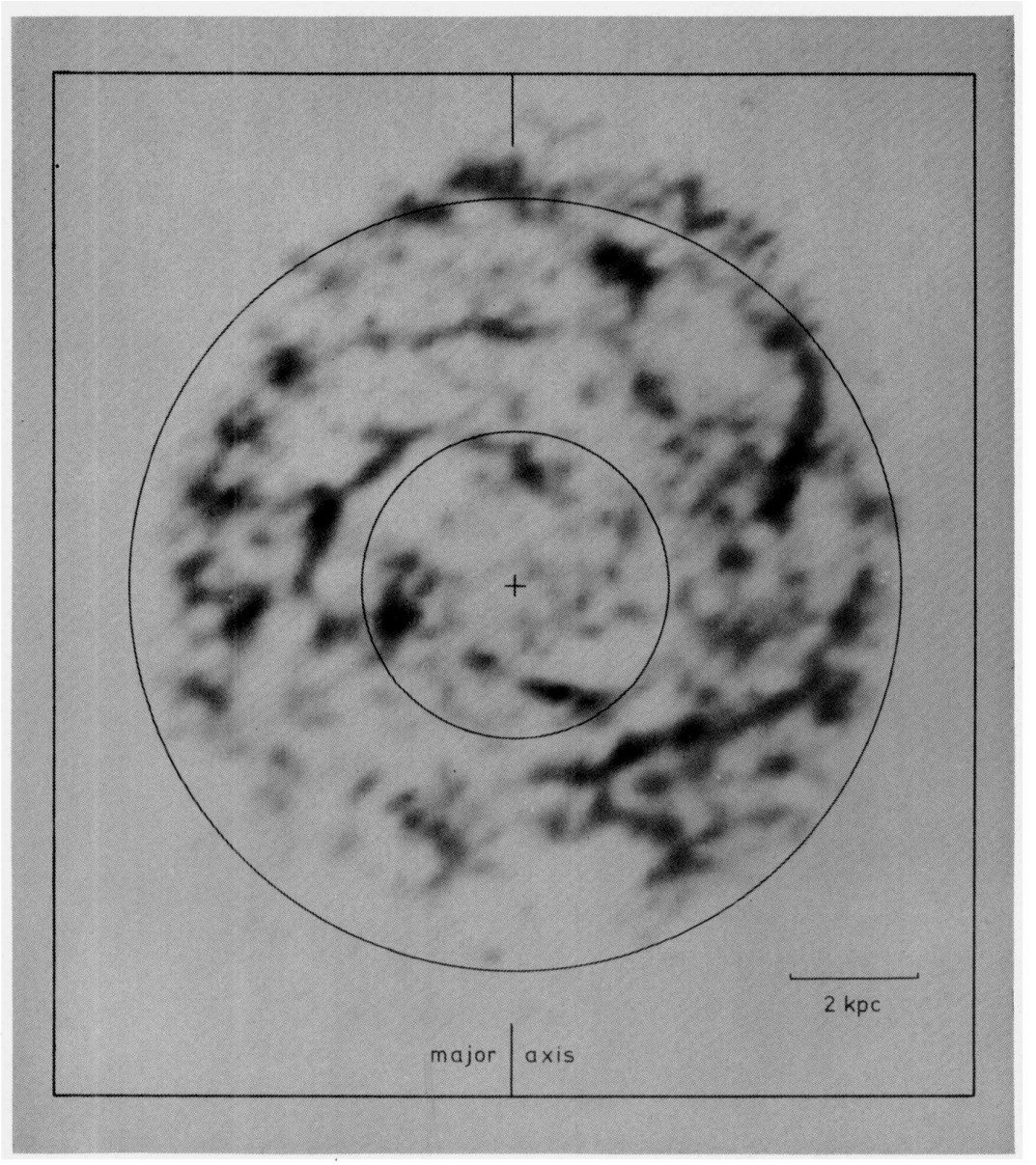

Plate 2. Map of the H I surface density deprojected to a face-on orientation in the plane of M33 (see text). Circles are shown at radii of 2.4 and 6 kpc.

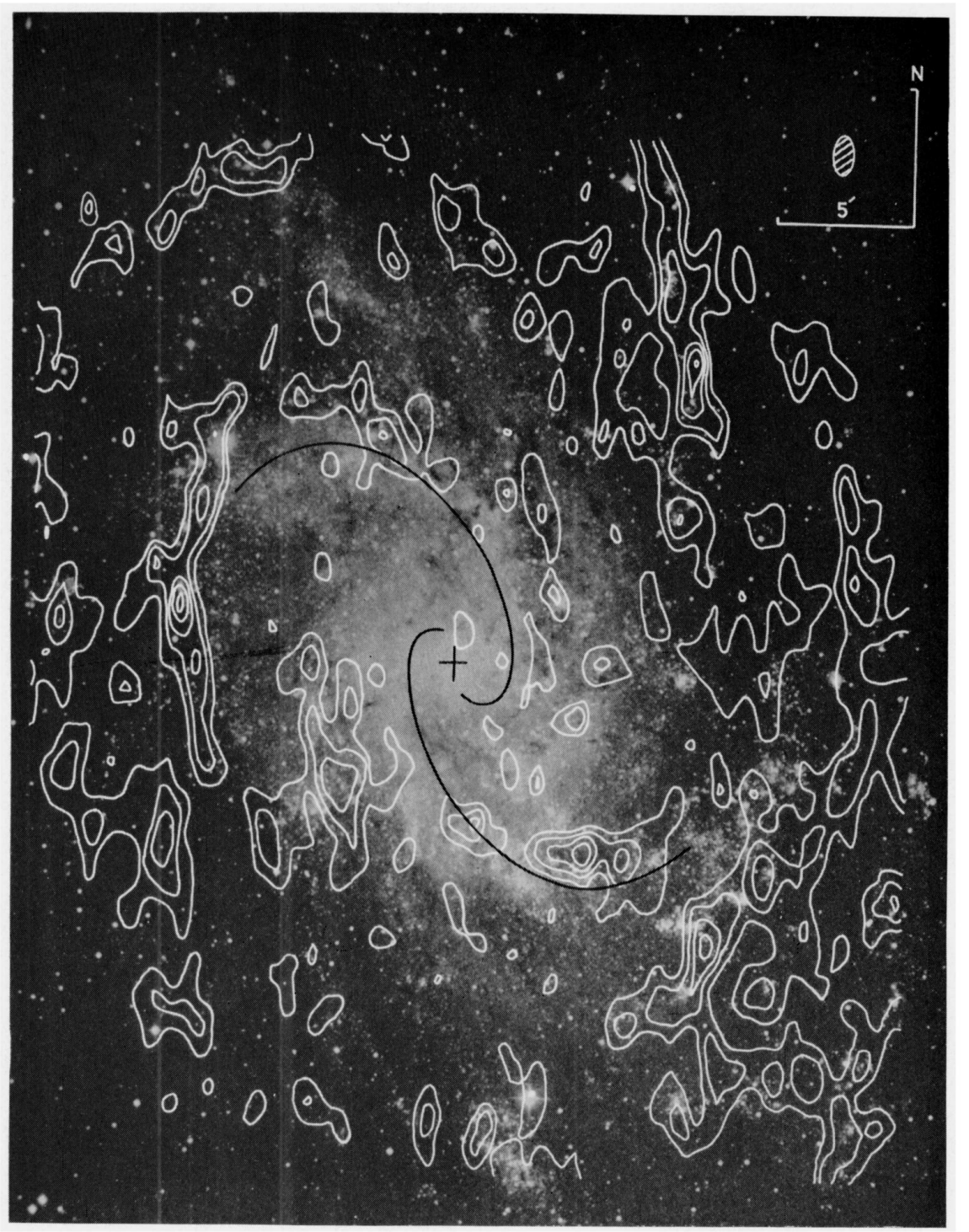

Plate 3. Photograph of M33 taken in blue light (Hubble Atlas) with peak contours of integrated H I emission superimposed. The contour interval is 291 K km s^{-1} and the first contour is at 872 K km s^{-1}. The solid curve is the logarithmic spiral shown on Fig. 1 and follows the two most prominent optical arms.

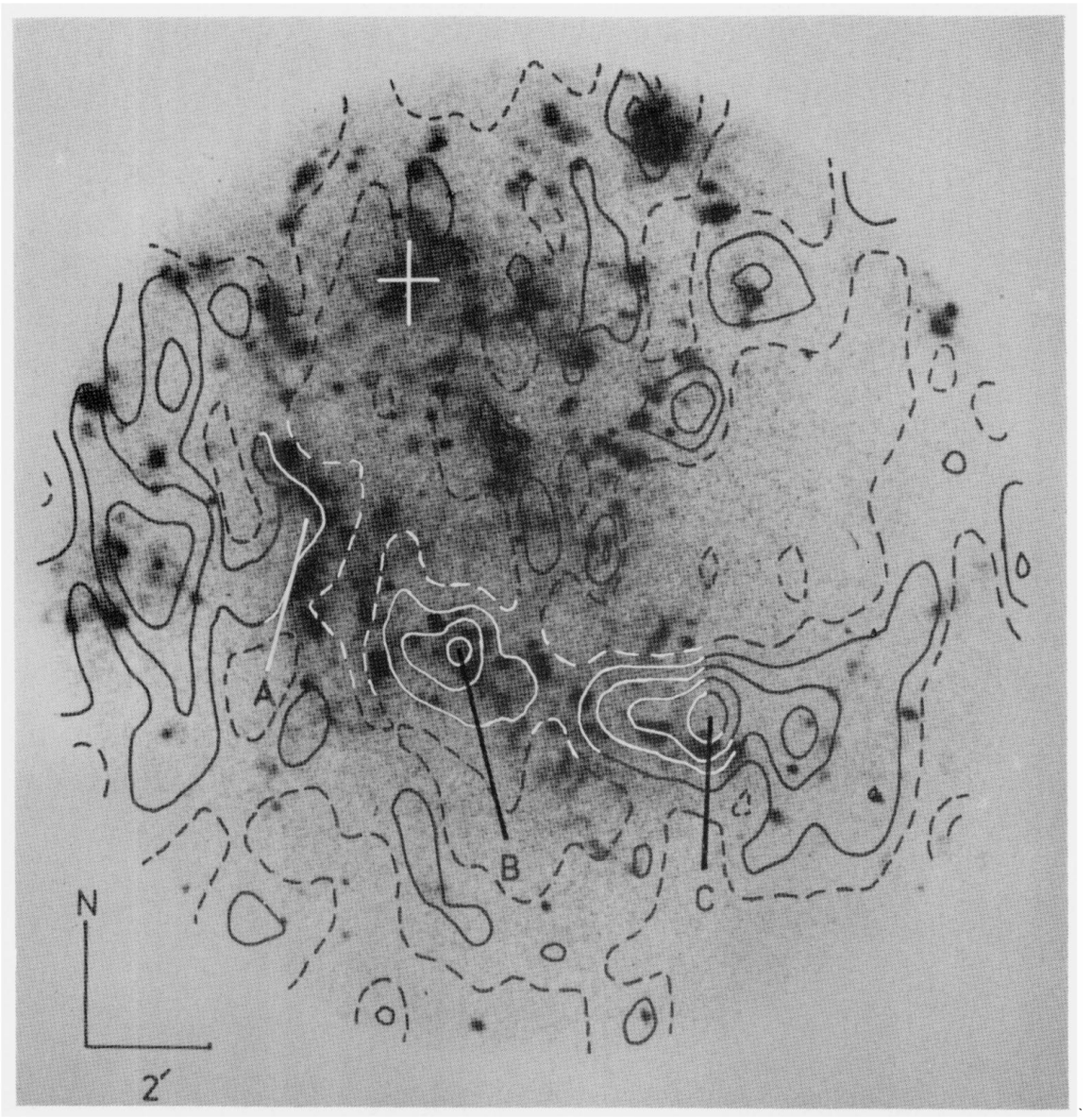

Plate 4. Contours of integrated H I emission at 47 × 93 arcsec resolution superposed on a Hα photograph of the inner southern arm in M33. Permission from *Astronomy and Astrophysics* to reproduce the photograph (Dubout-Crillon 1977) is gratefully acknowledged. The contour interval is 291 K km s^{-1} and the dashed contour is at 581 K km s^{-1}.

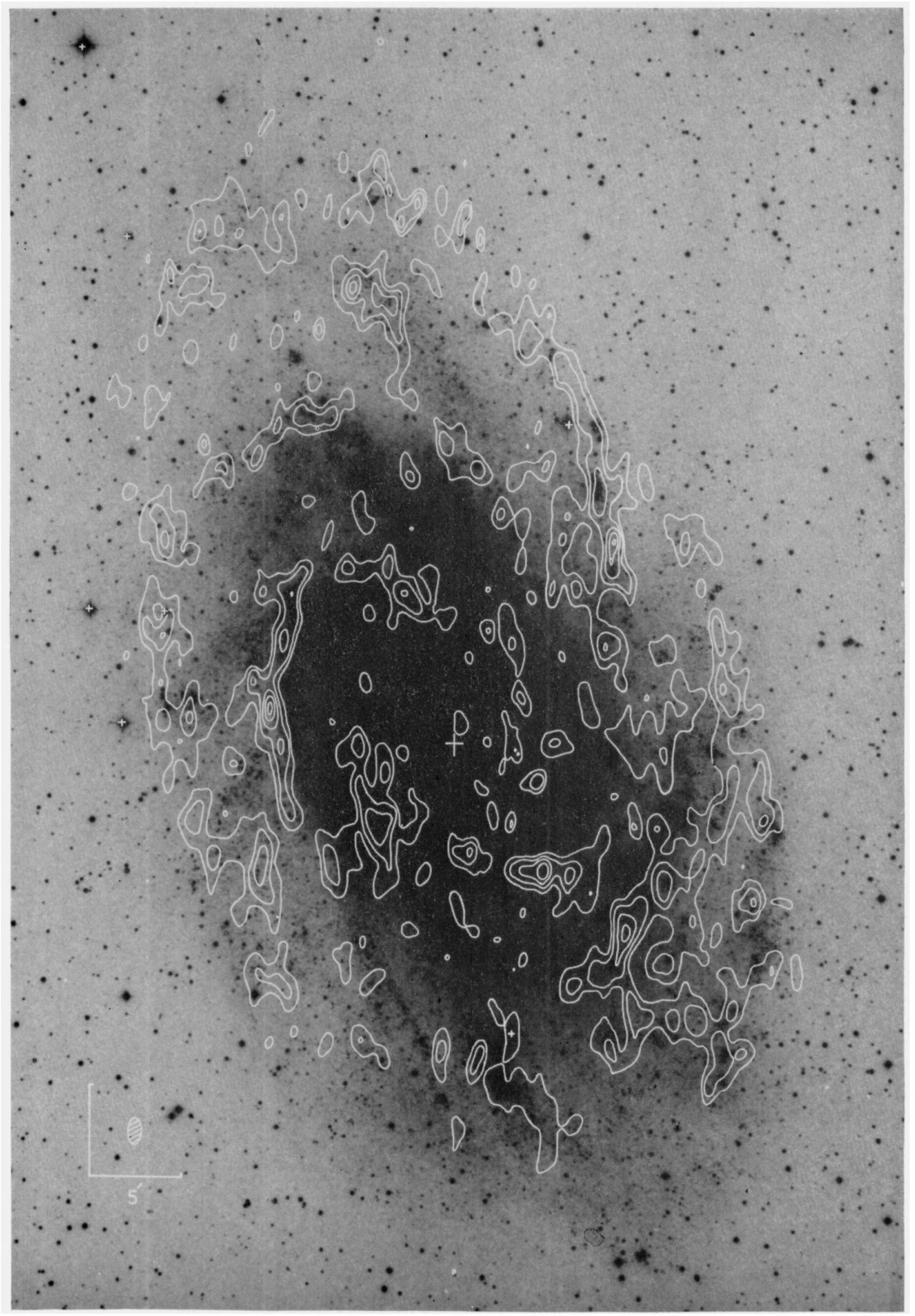

Plate 5. Peak contours of integrated H I emission at 47 × 93 arcsec resolution superposed on an optical photograph taken in blue light. The contour interval is 291 K km s^{-1}, starting from 872 K km s^{-1}. Photograph copyright by the National Geographic Society–Palomar Observatory Sky Survey. Reproduced by permission from the Hale Observatories.

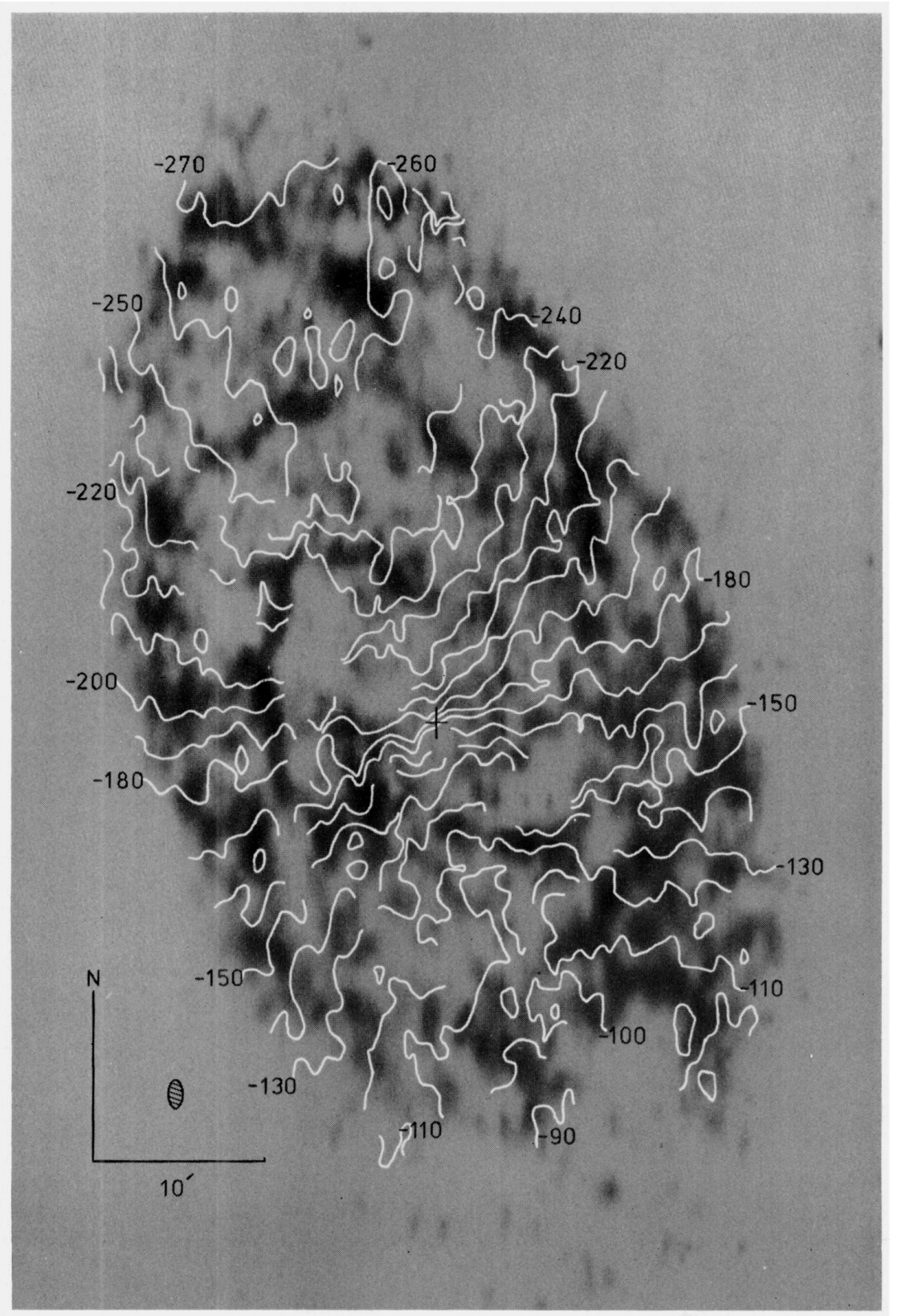

Plate 6. The radial-velocity map of M33, at 47 × 93 arcsec resolution superposed on an optical representation of the integrated H I emission. The contour interval is 10 km s^{-1}.

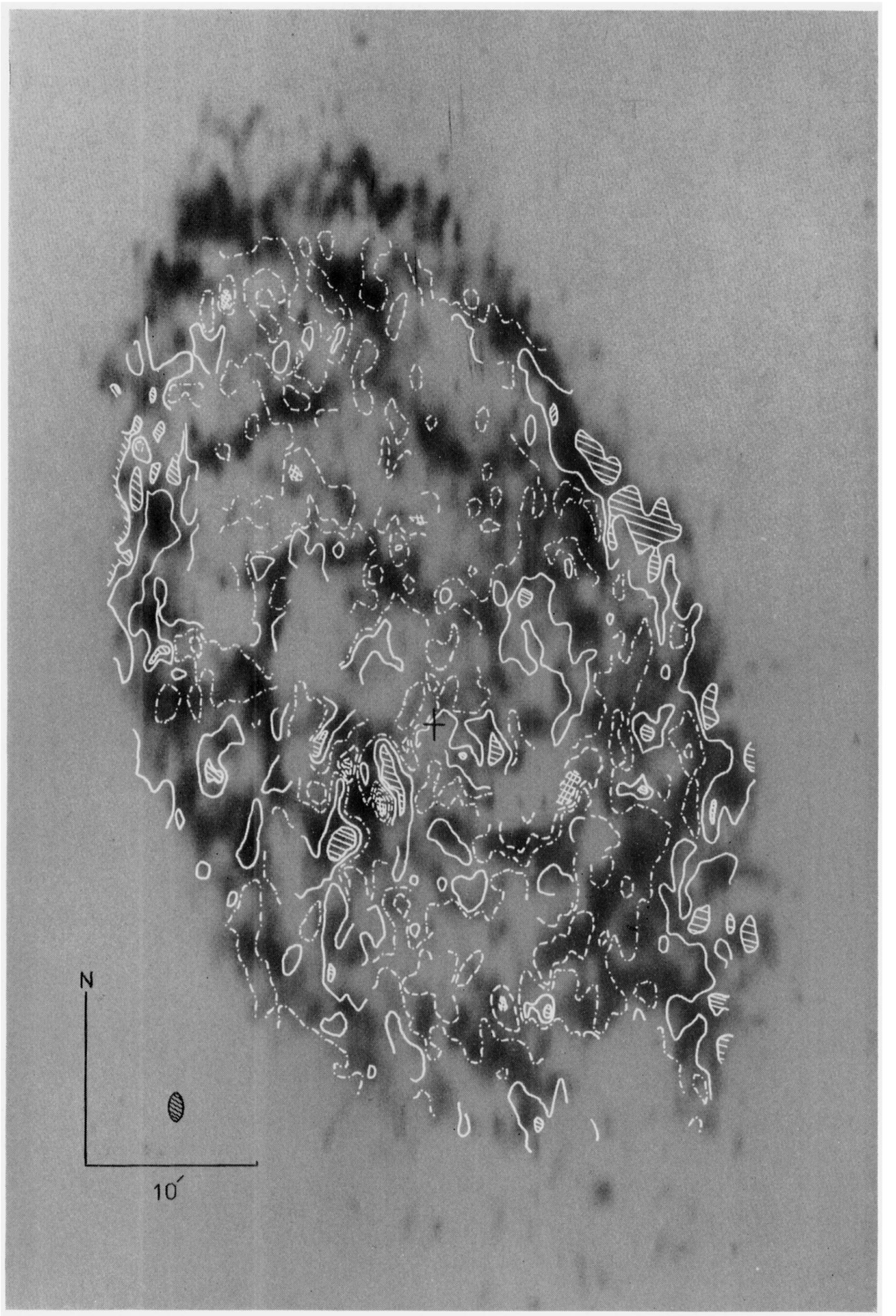

Plate 7. M33: residual velocity field. This shows the result of subtracting the velocities calculated from a flat disc model from the observed radial-velocity field at 47×93 arcsec resolution for $R \leqslant 6$ kpc. < -10 km s^{-1} cross-hatching; -5 km s^{-1} – – –; 0 km s^{-1} –·–·; 5 km s^{-1} ———; > 10 km s^{-1} single shading.

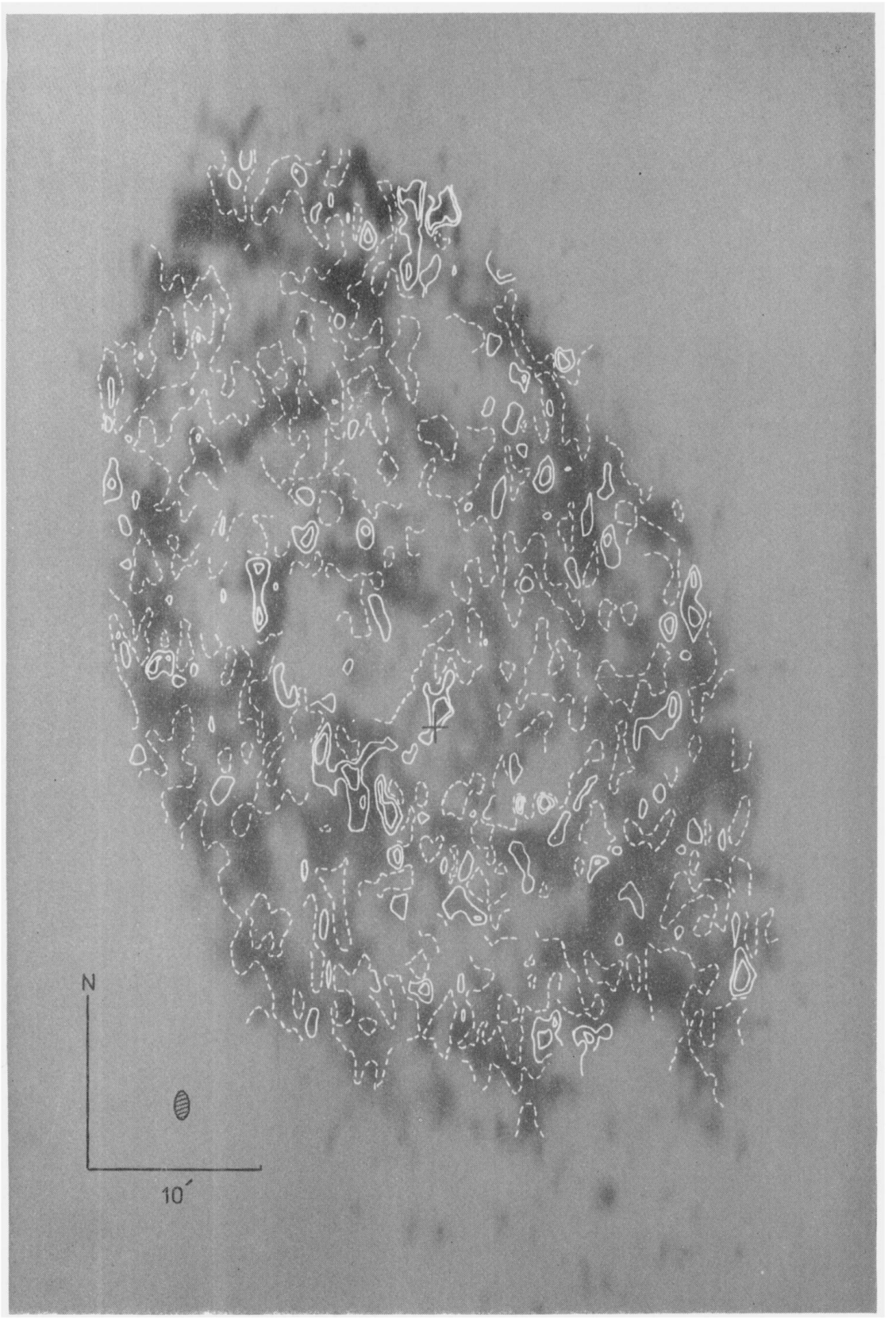

Plate 8. M33: A map of the observed dispersion (FWHP uncorrected for the 16-km s^{-1} instrumental bandwidth) of the H I profiles from the data at 47×93 arcsec resolution, superposed on an optical representation of the integrated emission. Contours are shown at 25 (dashed), 35 and 45 km s^{-1}.

of large-scale warping (Reakes & Newton 1978) may well be significant near the edge of the disc.

On the assumption that spiral features in M33 are part of a quasi-stationary density-wave pattern, an estimate of the magnitude of perturbations in the radial component of velocity inside an arm may be derived as follows. Consider a *narrow* arm, forming part of a stationary density-wave pattern in a frame rotating with angular velocity Ω_p. The radial component V_R of gas velocity in the disc relative to the arm is given by

$$(V_R)_{disc} \cong R[\Omega_p - \Omega(R)] \tan t,$$

where R is the distance to the centre, $\Omega(R)$ the gas rotational velocity and t the pitch angle of the spiral. Assuming σV_R to be constant along any streamline, where σ is the gas density, we have

$$\sigma_{arm}(V_R)_{arm} = \sigma_{disc}(V_R)_{disc}.$$

The perturbation of gas velocity inside the arm

$$V_r = (V_R)_{disc} - (V_R)_{arm}$$

is therefore given by

$$V_r \cong (1 - \sigma_{disc}/\sigma_{arm})\, R[\Omega_p - \Omega(R)] \tan t.$$

The resulting observed perturbation is

$$(V_r)_{obs} = V_r \sin i \sin \theta,$$

where i is the inclination of the disc and θ the angle in the plane of the disc measured relative to the major axis. Table 2 shows values of $V_r \sin i$ calculated for different radii and pattern speeds in M33, assuming $\sigma_{disc}/\sigma_{arm} = 0.3$, $t = 27°$ and $i = 54°$.

Estimates of the pattern speed (Ω_p) and hence corotation radius (R_c) of a spiral density-wave in M33 have been derived in several different ways and cover a wide range of values. The present survey, having mapped H I spiral arms in the outer parts of the disc, allows the problem to be approached in a new way. If the outer H I arm pattern rotates 'rigidly', it can

Table 2. Predicted amplitudes of the radial components of velocity perturbations along a narrow spiral arm in M33, derived for various possible corotation radii assuming the parameters given in the text. Negative values correspond to an apparent radial contraction of gas in the arm relative to the interarm gas.

Radius (kpc)	$V_r \cdot \sin i$ (km/s)			
Corotation radius =	1	2.4	4	6 kpc
	5	12	20	30 arcmin
Ω_p =	62	37	25.5	18 km/s·kpc
1	0.0	-7.0	-10.5	-12.7
2	11.3	-3.3	- 9.8	-14.1
3	26.3	4.8	- 5.3	-11.8
4	42.1	13.5	0.0	- 8.6
5	58.9	22.8	6.2	- 4.6
6	76.3	33.1	13.1	0.0

be seen from Table 2 that large radial streaming motions are expected along the outer arms if corotation occurs at a small radius. Feature 6 is the brightest arm near the minor axis in the outer part of the disc and would be expected to show the largest perturbation. The average residuals along the arm are 5 km s^{-1}, reaching to 10 km s^{-1} at the northern end, and they correspond to velocities inward toward the nucleus relative to interarm gas. From the table, with corotation at $R = 2.4$ kpc (the value estimated by Rogstad *et al.* 1976 from the H I distribution at 2-arcmin resolution), perturbations would be expected of order 20 km s^{-1} towards the end of feature 6 ($R > 5$ kpc) but with the opposite sense to the smaller perturbations observed. These perturbations would be smoothed by the synthesized beam and may be complicated by large-scale warping of the outer disc but, if the spiral pattern in the outer parts of M33 is 'quasi-stationary' with a pattern speed corresponding to corotation near $R = 2.4$ kpc, it is surprising that corresponding velocity perturbations are not observed. If the spiral features are indeed trailing, the simplest way to account for the absence of such large perturbations is to place corotation at a much larger radius.

From Table 2, predicted perturbations are relatively small for $R_c > 4$ kpc, i.e. $\Omega_p < 25$ km s^{-1} kpc^{-1} and would be close to zero for $R_c = 6$ kpc ($\Omega_p \simeq 18$ km s^{-1} kpc^{-1}). Such small values for the pattern speed are not unreasonable in view of the results derived from optical studies of the inner southern arm. Courtès & Dubout-Crillon (1971) suggest a small value of Ω_p (= 15 km s^{-1} kpc^{-1}) by considering the difference in age between the front and rear edges of the arm, with limiting values of $7 < \Omega_p < 25$ km s^{-1} kpc^{-1}. More recently, Boulesteix (communicated to Dubout-Crillon 1977) has determined $\Omega_p = 20$ km s^{-1} kpc^{-1} as the most probable value.

These observations therefore suggest that, if the outer spiral pattern in M33 indeed rotates 'rigidly' it does so with a pattern speed < 25 km s^{-1} kpc^{-1}, placing corotation in the outer parts of the disc. This upper limit may be compared with the values $\Omega_p = 18$ km s^{-1} kpc^{-1} adopted for M81 by Visser (1978) and 11 km s^{-1} kpc^{-1} for M31 by Guibert (1974).

The dynamics of the spiral arms in M33 are certainly more complex than, for example, M81 or M51 where, even on a larger linear scale, well-defined and bisymmetrical spiral patterns dominate the disc and observations are in good agreement with density-wave theories (Mathewson, van der Kruit & Brouw 1972; Roberts 1975; Visser 1978). It is unlikely that any simple density-wave model can account for the irregular and multi-armed spiral pattern in M33. If the arms are indeed wave-like phenomena, it seems reasonable to suppose that several density-wave modes may be present in the disc; such a possibility is not ruled out theoretically (e.g. Lin & Shu 1967), but as Shane & Bystedt (1978) point out, so many free parameters could be introduced as to make detailed model-fitting meaningless. If the arms are quasi-stationary waves, the calculations presented above predict that velocity perturbations would be measurable at the linear scale of the present survey, by observations with increased sensitivity and velocity resolution.

6.4 SHOCK-WAVES IN THE INTERSTELLAR GAS

Following the calculation presented above, the component of the underlying rotation velocity perpendicular to an arm which is stationary in a frame rotating with angular velocity Ω_p is given by

$$(V_\perp)_{\text{disc}} = R(\Omega_p - \Omega(R)) \sin t.$$

A shock would be expected when a supersonic–subsonic transition in $V_\perp$ occurs across the arm (e.g. Roberts *et al.* 1975). Using the symbols defined in Section 6.3,

$$(V_\perp)_{\text{arm}} = (\sigma_{\text{disc}}/\sigma_{\text{arm}})(V_\perp)_{\text{disc}}.$$

Table 3. Component of velocity perpendicular to a quasi-stationary spiral arm for various possible pattern speeds, derived by assuming the parameters given in the text. Negative values correspond to velocities away from the nucleus.

Radius (kpc)	Pattern speed (km/s.kpc) 62		37		25.5		18	
	$(V_\perp)_{disc}$	$(V_\perp)_{arm}$	$(V_\perp)_{disc}$	$(V_\perp)_{arm}$	$(V_\perp)_{disc}$	$(V_\perp)_{arm}$	$(V_\perp)_{disc}$	$(V_\perp)_{arm}$
1	0 km/s	0 km/s	-10.9	-3.3	-16.2	-4.9	-19.6	-5.9
2	17.6	5.2	- 5.1	-1.5	-15.6	-4.7	-22.4	-6.7
3	41.5	12.5	7.5	2.3	- 8.2	-2.5	-18.4	-5.5
4	66.7	20.0	21.2	6.4	0.3	0.1	-13.3	-4.0
5	92.7	27.8	35.9	10.8	9.8	2.9	-7.2	-2.2
6	120.0	36.0	52.0	15.6	20.7	6.2	0	0

Table 3 gives values of $(V_\perp)_{disc}$ and $(V_\perp)_{arm}$ calculated for different radii and pattern speeds, assuming $\sigma_{disc}/\sigma_{arm} = 0.3$ and $t = 27°$. Larger values of $(V_\perp)_{disc}$ are derived here than by Roberts *et al.*, partly due to the larger pitch angle adopted in the present calculation and partly because the calculation is extended beyond the corotation radius.

The effective acoustic speed of the interstellar gas was estimated as 7–12 km s^{-1} by Roberts *et al.*; assuming such values, Table 3 indicates that shocks are indeed possible in M33, although over different ranges of radii for different pattern speeds. Narrow H I features occur over the range $R \simeq 1.5$–6 kpc (Plate 1) and it may be seen from Table 3 that weak shocks would be expected over the largest range of radii for the lower pattern-speeds.

It is therefore possible that the narrow width of the H I spiral features can be explained in the density-wave picture as a result of weak shocks in the interstellar gas. Confirmation of the presence of such shocks would be strong support for the density-wave explanation. At present, however, there is no evidence either from optical or radio continuum observations for shocks in M33 anywhere other than the inner southern arm (Dubout-Crillon 1977, Section 5.2.1), and a detailed investigation of star formation along the outer H I arms would be useful to pursue this possibility further. For weak shocks, the shock-profile of both radial velocity and H I surface density (Roberts 1969) would be smoothed over the beam of the present survey and observations with higher angular resolution would be required to determine better profiles and compression ratios.

6.5 VELOCITY DISPERSION

Plate 8 is a map of the observed *dispersion* (defined as FWHP, uncorrected for instrumental broadening) of the H I profiles from the data at 47 x 93 arcsec resolution. Dispersions at points on the spiral features are generally similar to those measured in the interarm regions. There are high dispersions in the south-east interarm complex (feature 4 on Fig. 4) and they are associated with anomalies in the velocity field. From their data at lower resolution, Wright *et al.* (1972) found corrected dispersions varying from 36 km s^{-1} near the nucleus to 22 km s^{-1} at $R = 6$ kpc. The high values near the centre are often associated with regions which, in the present survey, are found to have anomalous velocities or high velocity-gradients. After omitting such regions, and allowing for beam-smoothing, dispersions are approximately constant with radius, having an average value of 23 ± 6 km s^{-1} from measurements along the major and minor axes. This corresponds to a rms value of 9 ± 3 km s^{-1}, in good agreement with values obtained for other spiral galaxies, e.g. our own Galaxy in the

neighbourhood of the Sun (7 km s^{-1}, van Woerden 1967), M31 (inner regions: 11.7 ± 1.3 km s^{-1}, Emerson 1976; outer regions: 9.7 km s^{-1}, Newton & Emerson 1977) and IC 342 (9.7 km s^{-1}, Newton, in preparation).

7 Conclusions

The most important results of the survey are summarized here.

(1) The H I distribution in M33 is clearly resolved into spiral features having typical lengths of 4 kpc and arm–interarm density–contrast ratios of 3.3 : 1. Spiral structure extends over most of the disc, and the best-defined features lie beyond the brightest optical arms. The H I spiral pattern is irregular and multi-armed; the arms are extremely narrow and frequently unresolved in width, implying true widths less than 160 pc.

(2) The peak brightness-temperatures observed in a 16-km s^{-1} bandwidth with 47 x 93 arcsec angular resolution are 55 K. The brightest peaks of integrated H I emission lie in the range 1400–2000 K km s^{-1}.

(3) There is excellent correlation between H I, optical emission and the position of H II regions. In the central areas, H I peaks are well correlated with dust lanes, and obscuration probably accounts for the tendency of observed H II regions to cluster around these inner peaks.

(4) The best direct evidence for the existence of a density-wave in M33 remains that derived from the morphology of the inner southern arm. The location of H I relative to other Population I material is in good agreement with predictions of the non-linear density-wave theory (Roberts & Yuan 1970) and supports the evidence presented by Dubout-Crillon (1977) for the presence of a shock-front associated with a density-wave in the arm. There is, however, no evidence for a symmetrical density-wave associated with the northern arm.

(5) There are velocity perturbations associated with the inner spiral arms near the major axis which are in qualitative agreement with predictions of the density-wave theory but which, depending on the distribution of material in the arms, may simply arise from the self-gravity of massive arms whether or not they are quasi-stationary waves. The absence of large perturbations along spiral arms near the minor axis in the outer parts of the galaxy can only be explained by the simple density-wave model (with 'rigid' rotation of the arms) if corotation occurs at a much larger radius (i.e. > 4 kpc) than suggested by Rogstad *et al.* (1976) from observations of the inner region. The implied limit on pattern speed ($\Omega_p < 25$ km s^{-1} kpc^{-1}) is consistent with values derived from optical studies of the inner southern arm (Courtès & Dubout-Crillon 1971).

Acknowledgments

I am grateful to many members of the Radio Astronomy Group for assistance with the observations and data analysis. I particularly thank Mr P. J. Warner, Drs J. E. Baldwin and J. R. Shakeshaft for helpful advice and discussion. Financial support from the Science Research Council and the Royal Commission for the Exhibition of 1851 is gratefully acknowledged. I also thank an anonymous referee for constructive comments on the presentation of this paper.

References

Berkhuijsen, E. M., 1977. *Astr. Astrophys.*, **57**, 9.
Boulesteix, J., Courtès, G., Laval, A., Monnet, G. & Petit, H., 1974. *Astr. Astrophys.*, **37**, 33.

Courtès, G. & Dubout-Crillon, R., 1971. *Astr. Astrophys.*, **11**, 468.
de Vaucouleurs, G. H., de Vaucouleurs, A. & Corwin, H. G., Jr., 1976. *Second Reference Catalogue of Bright Galaxies.* University of Texas Press, Austin.
Dixon, M. E., 1971. *Astrophys. J.*, **164**, 411.
Dubout-Crillon, R., 1977. *Astr. Astrophys.*, **56**, 293.
Emerson, D. T., 1974. *Mon. Not. R. astr. Soc.*, **169**, 607.
Emerson, D. T., 1976. *Mon. Not. R. astr. Soc.*, **176**, 321.
Guibert, J., 1974. *Astr. Astrophys.*, **30**, 353.
Israel, F. P. & van der Kruit, P. C., 1974. *Astr. Astrophys.*, **32**, 363.
Kalnajs, A. J., 1978. *IAU Symp. No. 77*, p. 113., eds Berkhuijsen, E. M. & Wielebinski, R., Reidel, Dordrecht, Holland.
Lin, C. C. & Shu, F. H., 1967. *IAU Symp. No. 31*, p. 313.
Lin, C. C., Yuan, C. & Shu, F. H., 1969. *Astrophys. J.*, **155**, 721.
Madore, B. F., 1978. *Observatory*, **98**, 169.
Madore, B. F., van den Bergh, S. & Rogstad, D. H., 1974. *Astrophys. J.*, **191**, 317.
Mathewson, D. S., van der Kruit, P. C. & Brouw, W. N., 1972. *Astr. Astrophys.*, **17**, 468.
Newton, K., 1978 *PhD thesis*, University of Cambridge.
Newton, K. & Emerson, D. T., 1977. *Mon. Not. R. astr. Soc.*, **181**, 573.
Reakes, M. L. & Newton, K., 1978. *Mon. Not. R. astr. Soc.*, **185**, 277.
Roberts, W. W., 1969. *Astrophys. J.*, **158**, 123.
Roberts, W. W., 1975. *La Dynamique des Galaxies Spirales*, p. 115, Centre National de la Recherche Scientifique, Paris.
Roberts, W. W., Roberts, M. S. & Shu, F. H., 1975. *Astrophys. J.*, **196**, 381.
Roberts, W. W. & Yuan, C., 1970. *Astrophys. J.*, **161**, 887.
Rogstad, D. H., Wright, M. C. H. & Lockhart, I. A., 1976. *Astrophys. J.*, **204**, 703.
Rots, A. H. & Shane, W. W., 1975. *Astr. Astrophys.*, **45**, 25.
Shane, W. W. & Bystedt, J., 1978. *IAU Symp. No. 77*, p. 97. eds Berkhuijsen, E. M. & Wielebinski, R., Reidel, Dordrecht, Holland.
Toomre, A., 1977. *A. Rev. Astr. Astrophys.*, **15**, 437.
van der Kruit, P. C., 1973. *Astr. Astrophys.*, **29**, 231.
van Woerden, H., 1967. *IAU Symp. No. 31*, p. 3. ed. van Woerden, H., Academic Press, New York.
Visser, H. C. D., 1978. *PhD thesis*, University of Groningen.
von Kap-herr, A., Berkhuijsen, E. M. & Wielebinski, R., 1978. *Astr. Astrophys.*, **62**, 51.
Warner, P. J., Wright, M. C. H. & Baldwin, J. E., 1973. *Mon. Not. R. astr. Soc.*, **163**, 163.
Winter, A. J. B., 1975. *Mon. Not. R. astr. Soc.*, **172**, 1.
Wright, M. C. H., Warner, P. J. & Baldwin, J. E., 1972. *Mon. Not. R. astr. Soc.*, **155**, 337.